N. Oláh et al. / Ceramics International 41 (2015) 5863–5871

Sputtered nanocrystalline TiC / amorphous C thin films as potential materials for medical applications

Nikolett Oláh[1], Zsolt Fogarassy[1], Mónika Furkó[2], Csaba Balázsi[2], Katalin Balázsi[1*]

[1] *Thin Film Physics Department, Institute for Technical Physics and Materials Science, Research Centre for Natural Sciences, Hungarian Academy of Sciences, Konkoly-Thege M. str. 29-33, 1121 Budapest, Hungary*
[2] *Institute for Materials Science and Technology, Bay Zoltán Nonprofit Ltd for Applied Research, Fehérvári str. 130, 1116 Budapest, Hungary*

**balazsi.katalin@ttk.mta.hu, balazsi@mfa.kfki.hu*

Abstract

The relationship between structural behaviour of sputtered TiC / amorphous C (TiC /a:C) thin films and corrosion properties was measured in three various pH solutions (0.5 M NaCl (pH=6); 0.1 M HCl (pH=1); 0.1 M NaOH (pH=13). The ~ 400 nm thick nanocomposites were deposited by DC magnetron sputtering on different substrates (Ti6Al4V alloy and CoCrMo alloy) in argon at 25 C° and 0.25 Pa with 150 W input power of carbon target and 50 W input power of titanium target. The structure and composition of nanocomposites were investigated by Transmission and Scanning Electron Microscopy. In both samples the structural investigations confirmed columnar structure of TiC /a:C films with 25-50 nm sized cubic TiC. These columns were separated by 2 - 3 nm thin amorphous carbon layers. TiC /a:C /Ti6Al4V alloy implant material showed better corrosion resistance than the TiC /a:C /CoCrMo alloy in 0.5 M NaCl solution based on results of the Electrochemical Impedance Spectroscopy. For both samples, the 0.1 M NaOH solution was the most corrosive media.

1. Introduction

CoCrMo and Ti6Al4V alloys are widely used as medical implants. These alloys exhibit excellent corrosion resistance, biocompatibility, high durability and strength [1-3]. Pure titanium undergoes an allotropic transformation from the hexagonal close-packed (HCP) alpha phase structure to the body-centered cubic (BCC) beta phase structure at a temperature of 882 °C [4]. Due to this structural change titanium alloys fall into three classes: α alloys, α+β alloys and β alloys. Different alloying elements can stabilize either the α (for example aluminium) or β phase (for example vanadium) [4-5].

The release of V, Al, Ti, Co, Cr or Mo into adjacent tissue has been detected based on several previous studies [6-8]. Research on Ti6Al4V alloy showed corrosion problems [9]. This problem can be solved with proper pretreatments before implantation. There are several methods to modify the surface of implant materials including ion implantation [10], sand-blasting [11], the application of micro-rough Ti surfaces via Al_2O_3 sandblasting and acid etching (SLA), heat treatment and alkali treatment (SMART), hydrogen peroxide and heat treatment (SAOH), and potentiostatic anodization in sulfate electrolytes through constant

electric current supply (ECH) [12]. *H. B. Wen et al.* [13] also used a simple chemical treatment, namely incubation in diluted alkali at 140 °C, while *T. Hanawa* [14] examined the effect of calcium ion implantation into titanium. In both cases, Ca-P deposition or precipitation was observed on the substrates.

Biomaterials must be nontoxic, non-carcinogenic, chemically inert, stable and mechanically strong enough to withstand the repeated forces during their lifetime. These conditions are achievable with producing a protective film or surface coating on metal devices [15]. Nanocomposite coatings consisted of nanocrystalline grains and amorphous matrix promises possibility of synthesizing a surface protection layer with an unusual combination of mechanical properties [16]. Titanium carbide (TiC) may be a potential candidate for such a surface protection coating which serves as barrier layer because of its high mechanical hardness, excellent corrosion resistance and good biocompatibility [17-19]. The corrosion behaviour can be studied by potentiodynamic measurements and by Electrochemical Impedance Spectroscopy (EIS). EIS is a non-destructive and also one of the most appropriate techniques to characterize the corrosion behaviour of our materials [20].

In this work, the investigation of the composition and corrosion behaviour of the TiC /a:C coated and uncoated CoCrMo and Ti6Al4V alloys were studied by three solutions with different pH-s applied at room temperature: acidic hydrogen chloride with pH of 1, basic sodium hydroxide with pH of 13 and close to neutral sodium chloride with pH of 6. The comparison of structural changes before and after corrosion tests was examined.

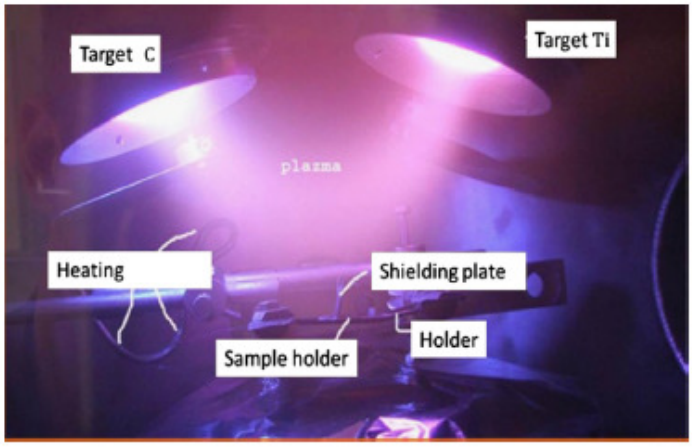

Fig. 1. Real image of DC magnetron sputtering equipment used for TiC/a:C thin films.

2. Material and methods

2.1. Purchased materials

The commercial Ti6Al4V and CoCrMo substrates were purchased from Protetim Ltd. with diameter 20 mm and thickness 2 mm. They were applied in this paper in “uncoated” (pristine) and “coated” forms. The coating procedure is described below. The commercial CoCrMo substrate are composed of 58.9-69.5 % Co, 27.30 % Cr, 5.0-7.0 % Mo and limits on other important elements such as Mn, Si, less than 1 % Fe, Ni and C [21]. One side (the one to

be coated) of the samples was roughened using a sandblasting procedure with a 180 grit aluminium oxide media for better cell adhesion.

2.2. Thin Film preparation

DC magnetron sputtering was used for deposition of ~ 400 nm thin TiC /a:C nanocomposite films on the above substrates at room temperature in argon 0.25 Pa (Fig. 1). The detailed preparation steps were described in our previous works [22]. The input power applied on the carbon target (99.999 %, Kurt and Lesker) was 150 W, while that applied for the titanium target (99.995 %, Kurt and Lesker) was 50 W. The sample-target distance was ~ 70 mm.

2.3. Structural characterization

All thin films were first mechanically thinned to ~ 50 μm. Then, they were further thinned till perforation by 6 kV Ar^+ ions from both sides. The thin damaged layer was removed by 2 keV Ar^+ ions. This procedure minimized the thermal load during sample preparation. Transmission Electron Microscopy (TEM, Philips CM-20, 200 kV) and High Resolution Electron Microscopy (HREM, JEOL 3010, 300 kV) equipped with and Electron Energy Loss Spectroscopy (EELS) were used for cross-sectional structural investigations of films and substrates. Surface morphologies of coated and uncoated substrates before and after corrosion tests were studied by Scanning Electron Microscopy (SEM-LEO 1540 XB). Selection Area Electron Diffraction (SAED) was used for the phase analysis.

2.4. Electrochemical tests

The potentiodynamic and electrochemical impedance measurements were carried out with Zahner IM6e electrochemical workstation (Zahner, Germany). The electrochemical potentiodynamic polarization tests were performed in a standard three-electrode-cell, at a potential scanning rate of 0.5 mV s^{-1} initiated at −200 mV below the open-circuit potential. During all measurements the atmosphere was open to air. The working electrodes were the metallic implant discs Ti6Al4V (ISO5832-3) and CoCrMo (ISO5832-12) with 1.37 cm^2 active surface area with ("coated") and without ("uncoated") TiC /a:C coating. Platinum net electrode was used as counter electrode. Ag /AgCl /KCl_{sat} electrode was used as reference electrode. The electrolyte was 0.5 M NaCl solution (pH=6), 0.1 M HCl solution (pH=1) and 0.1M NaOH solution (pH=13). The tests were started after a steady state open-circuit potential was attained (not more than ±5 mV drift within 5 min). The polarization curves were recorded after 30 min immersion time and they were characterized by the Tafel extrapolation method.

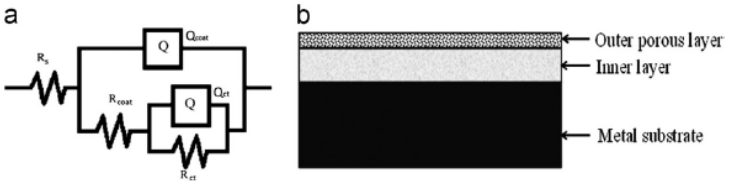

Fig. 2. Electrical equivalent measurements. (a) Electrical equivalent circuit used to simulate the measured data for TiC coated metallic implants, and (b) schematic of a proposed two-layer film formed on the surface of substrate, comprising of an inner layer and an outer porous layer.

EIS was measured by open circuit potential of the working electrode in 0.9 wt% NaCl solution at room temperature by applying a 10mV AC sine wave perturbation. During the EIS measurements, the frequency span was changed from 100 kHz down to 10 mHz. The investigated samples were initially immersed into solution and left at open-circuit for 30 min to stabilize the surface of specimen. EIS spectra were represented in both complex impedance diagrams (Nyquist plot) and Bode amplitude and phase angle plots. The imaginary component of the impedance is plotted as a function of the real component in the Nyquist graph, whereas the Bode representation shows the logarithm of the impedance modulus |Z| and phase angle ϕ as a function of the logarithm of the frequency (f). All impedance data were fitted and analyzed using Zview2 software. In each case, it was necessary to set up an appropriate equivalent circuit to estimate the values of charge transfer resistance (*R*ct). For this purpose, the impedance spectra were analysed using electrical equivalent circuit model is shown in Fig. 2a.

The most common form of circuit model is a two-time-constant model with resistances and capacitances related to each of the coating and the substrate (or interface). The coating layer formed on the implant materials can be considered as a two-layer coating, with an inner layer (oxide) and an outer unsealed porous (TiC) layer (Fig.2b). The equivalent circuit consists of the solution resistance connected in series with two parallel RC circuits. In this equivalent circuit, the high frequency time constant ($R_{coat}Q_{coat}$) is related to the contribution of TiC films to impedance response, associated with the penetration of the electrolyte through the pores, while the parallel-connected low frequency time constant $R_{ct}Q_{ct}$ are used to describe the charge transfer process at the substrate/coating interface through the pores, where R_{ct} represents the charge transfer resistance and Q_{ct} is the double layer capacitance of the substrate. R_S is an uncompensated solution resistance between the coating and the reference electrode. The impedance of a phase element is defined as $Z_{CPE} = 1/[Q(j\omega)^n]$, where the exponent n of the CPE is related to the non-equilibrium current distribution due to the surface roughness and surface defects. The CPE (which represents deviation from the true capacitor behaviour) is used here instead of an ideal double layer capacitance.

3. Results and discussion

3.1 Structural properties

3.1.1. Results on the CoCrMo substrate

The structural investigation of the uncoated substrate confirmed the co-existence of face-centered cubic (FCC) and the hexagonal closed-packed (HCP) cobalt crystalline structures in the CoCrMo substrate (Fig. 3). This result is in good agreement with the work of *Balagna et al.* [23]. The substrate consisted mainly of few micrometers Co crystalline grains (not shown). The TEM results of the structural characterization were analyzed by using of "ProcessDiffraction" program. This is a computer program to process electron diffraction patterns from polycrystalline or amorphous samples [24-27]. The cubic (Fig. 3a) and

hexagonal (Fig. 3b) Co grains were observed by Selection Area Electron Diffraction (SAED) images (Fig. 3). The cubic Co grains showed [011] orientation while the hexagonal grains had [01$\underline{1}$0] orientation. The Co and Cr atoms are usually oxidized rapidly at the surface and form the Cr_2O_3 oxide layer with less than 15 nm thicknesses [22, 28]. In our case, the oxide layer on the surface was not found.

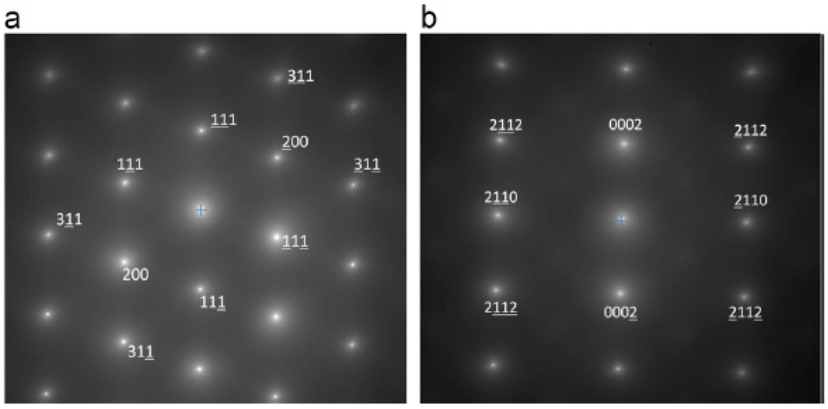

Fig. 3. SAED of uncoated CoCrMo substrate. (a) [011] Oriented Co cubic phase and (b) [01$\underline{1}$0] oriented Co hexagonal phase.

TEM studies of the TiC /a:C nanocomposite films proved the columnar structure of TiC crystals, embedded in the amorphous carbon matrix (Fig. 4a). The carbon interlayer was observed between the CoCrMo substrate and TiC/a:C thin film by EELS measurement (Fig. 4b). This interlayer was formulated at the beginning of sputtering process and it improved the adhesion of the TiC /a:C film. The average thickness of TiC columns were around 50 nm. The SAED showed the cubic phase of TiC crystals (Fig. 4c).

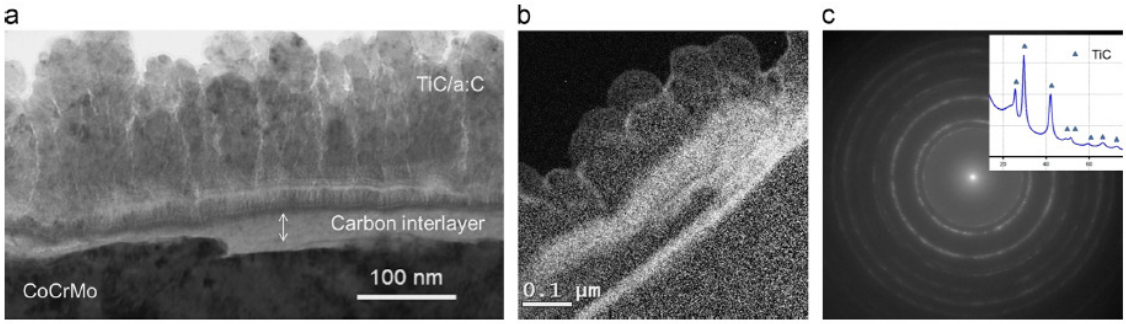

Fig. 4. TEM investigation of TiC/a:C coated CoCrMo implant. (a) Cross-sectional TEM image of the substrate with the coating on it (b) EELS map of carbon, and (c) SAED of cubic TiC with Miller indices (110),(200), (220), (311), (222), (400), (331), and (420).

3.1.2. Results on the Ti6Al4V substrate

The structural investigation of the sintered Ti6Al4V alloy confirmed mainly the presence of the α and β phases (Fig. 5), which is similar to the equiaxed microstructure found in a powder metallurgical matrix material [29, 30]. The major α-Ti phase is a hexagonal phase with (100), (002), (101), (102), (110) indices (JCPDFWIN 05-0682) (Fig. 5a, c). The second major phase is a cubic β - Ti phase with (110), (200), (211) indices (JCPDFWIN 44-1288) (Fig. 5a, d). The roughness of implant materials is one of their most important

properties, as the increasing roughness may increase their osseointegration and cell adhesion to them [30]. According to this point of view, the substrate was roughness enhanced by Al_2O_3 blasting. In our case, the diffraction peak of Al_2O_3 did not present.

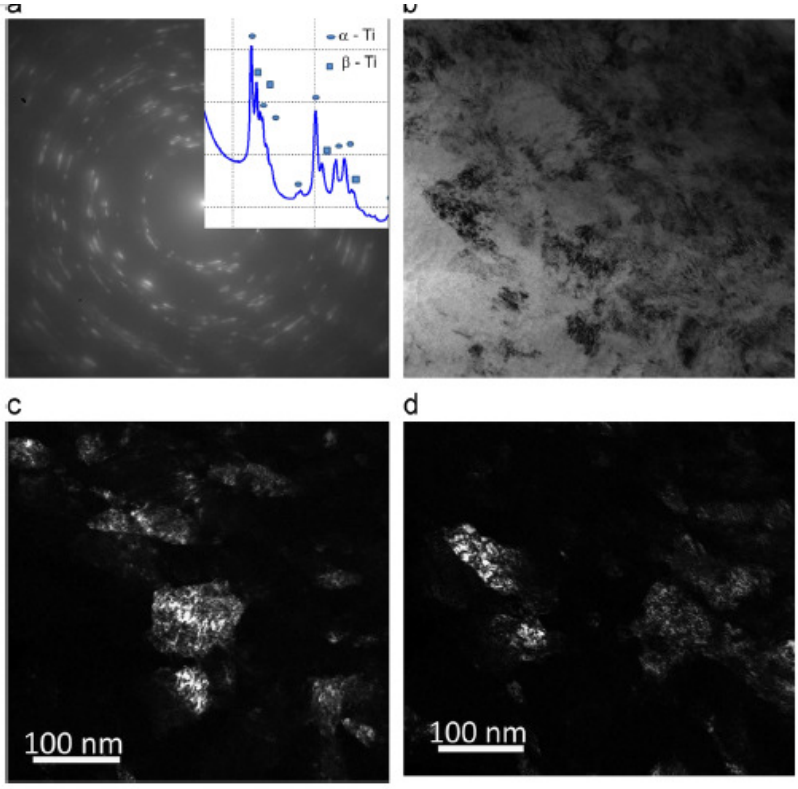

Fig. 5. TEM study of Ti6Al4V substrate. (a) SAED of Ti6Al4V substrate, (b) bright field TEM image of Ti6Al4V substrate, (c) dark field TEM imag phase, and (d) dark field TEM image of β-Ti phase.

TEM observations of TiC /a:C coating on Ti6Al4V substrate showed the columnar structure of TiC crystals (Fig. 6). The average width of columns is around 25 nm (Fig. 6a). It is half of the width compared to the TiC columns deposited on CoCrMo at the same deposition parameters. The columns are separated by 2 nm thin carbon matrix. The thickness of TiC /a:C thin films is ~ 400 nm. SAED confirmed only the presence of cubic TiC phase with (111) (200) (220) (311) (222) (400) indices (JCPDFWIN 32-1383) (Fig. 6b). As shown in Fig. 6c, the Al_2O_3 blasting grains did not form a continuous layer. The cross section study confirmed good adhesion of TiC layer on the substrate without any carbon or other interlayer between them, in contrary to the previous case (Fig. 4b).

3.2 Corrosion tests

3.2.1 Electrochemical test by Tafel analysis

In order to compare the susceptibility to corrosion of the TiC /a:C coated substrates relative to the uncoated ones, potentiodynamic polarization curves in three different solutions are shown in Fig 7. The corrosion potentials of TiC /a:C coated substrates are shifted to more positive potentials by about 150 – 400 mV compared with the uncoated substrates. In all cases, the corrosion potentials are shifted to more noble direction with increasing the pH values.

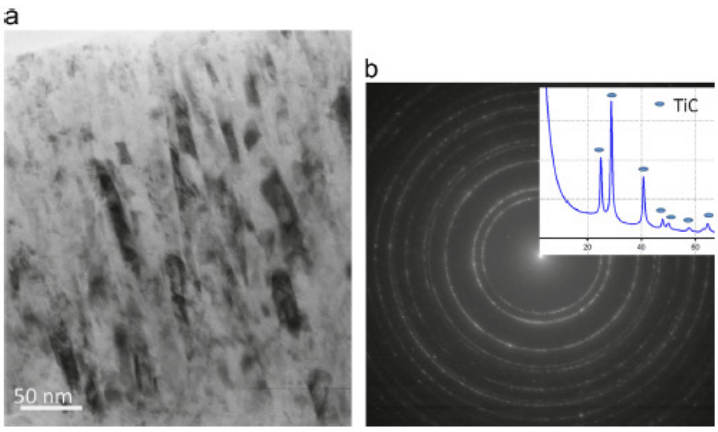

Fig. 6. TEM study of TiC coating on Ti6Al4V substrate. (a) Bright field cross section TEM image of TiC coating, (b) SAED of TiC coating, and (c) cross section TEM image of TiC/a:C and Ti6Al4V substrate interface.

Quantitative information of corrosion currents and corrosion potentials has been extracted from the slope of the curves, using the Stern-Geary equation (1). Corrosion resistance were related to the corrosion current density as:

$$i_{corr} = \frac{\beta a \times \beta c}{2.303 \times Rp \times (\beta a + \beta c)} \qquad (1)$$

where i_{corr} is the corrosion current density in A/cm^2; Rp is the corrosion resistance in ohms.cm^2; βa is the anodic Tafel slope in V/decade of current density; βc is the cathodic Tafel slope in V/decade of current density [31]. The Stearn–Geary equation illustrates the corrosion current as a value inversely proportional to charge transfer resistance. The corrosion current density is representative for the degradation degree of the alloy. The corrosion current (i_{corr}) for uncoated Ti6Al4V alloy was significantly lower than that of uncoated CoCrMo alloy as shown in work of *V. Swaminathan et al*. [20].

The highest corrosion current density was obtained in alkaline media (0.1 M NaOH), while the smallest values were found in the neutral, 0.5 M NaCl solution. The uncoated substrates showed 10 times lower corrosion current density (which is proportional to the corrosion rate) than the TiC /a:C coated implants in dependently of the type of substrate. The trend in the changing of corrosion rate can be explained by the formation of defects and pores in the coating. The structural investigations of films were in good agreement with corrosion tests. This study confirmed that the TiC /a:C coated implants have the highest corrosion rate

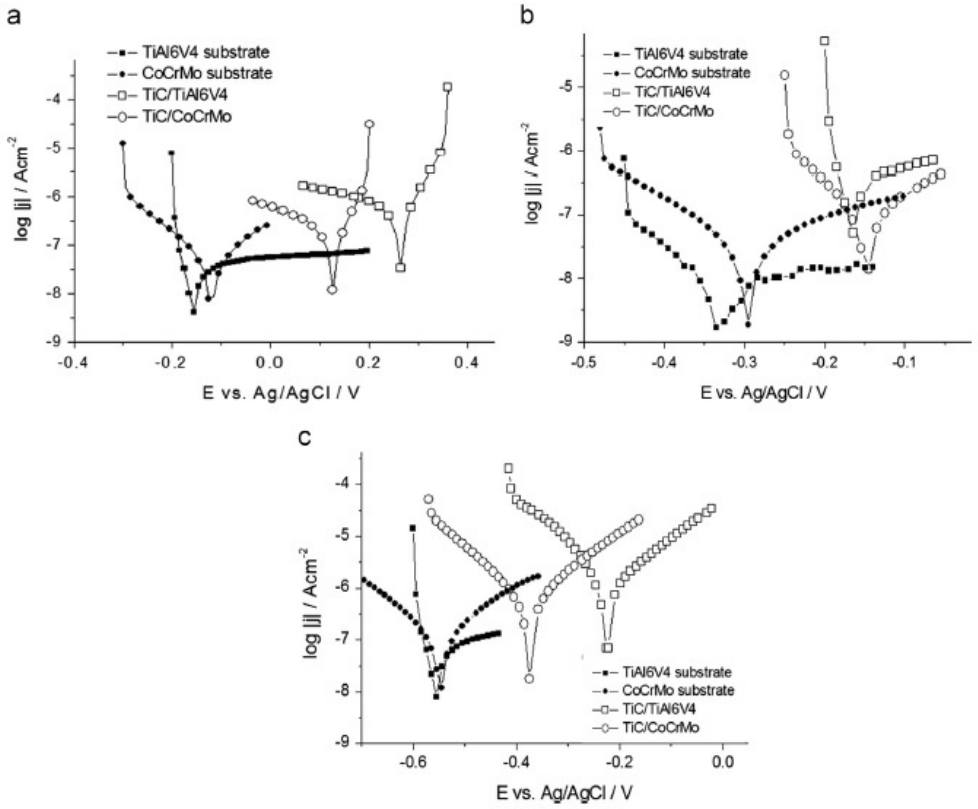

Fig. 7. Potentiodynamic measurements of TiC/a:C coated and uncoated substrates (Ti6Al4V and CoCrMo) in (a) 0.1 M HCl solution, (b) 0.5 M NaCl solution, and (c) 0.1 M NaOH solution.

due to their less dense structure. On the other hand, the Ti6Al4V implant alloy exhibited an excellent corrosion resistance, at the same time, titanium, aluminum and vanadium ions were found in the cell tissue by the way of the passive film dissolution [32]. Nevertheless, the TiC /a:C thin films with lower corrosion resistance are suitable as implant material.

3.2.2 Electrochemical Impedance Spectroscopy (EIS)

One of convenient ways to evaluate the corrosion properties of the samples is to compare the diameters of the semi-circles in Nyquist plot. Fig. 8 presents the Nyquist and Bode plots of TiC /a:C coated implant alloy at open circuit potentials (E_{ocp}).

It can be expected that the larger diameter of Nyquist plot referred to the higher corrosion resistance of the film. According to the EIS spectra, the diameters and the bending of the quasi-semicircles Nyquist plots revealed the most prone corrosion in 0.1 M NaOH solution compared with the measurements in 0.5 M NaCl solution and in the 0.1 M HCl. The

highest surface resistance was observed in 0.5 M NaCl solution in the case of Ti6Al4V and CoCrMo substrates, too. On the other hand, *R. Wen* [33, 34] showed the aggressive chloride ion will enhance the corrosion of metallic implant alloys. From this point of view, TiC /a:C deposited by DC magnetron sputtering on different substrates are suitable as material for corrosive medium. The potentiodynamic measurements were in a good agreement with EIS spectra.

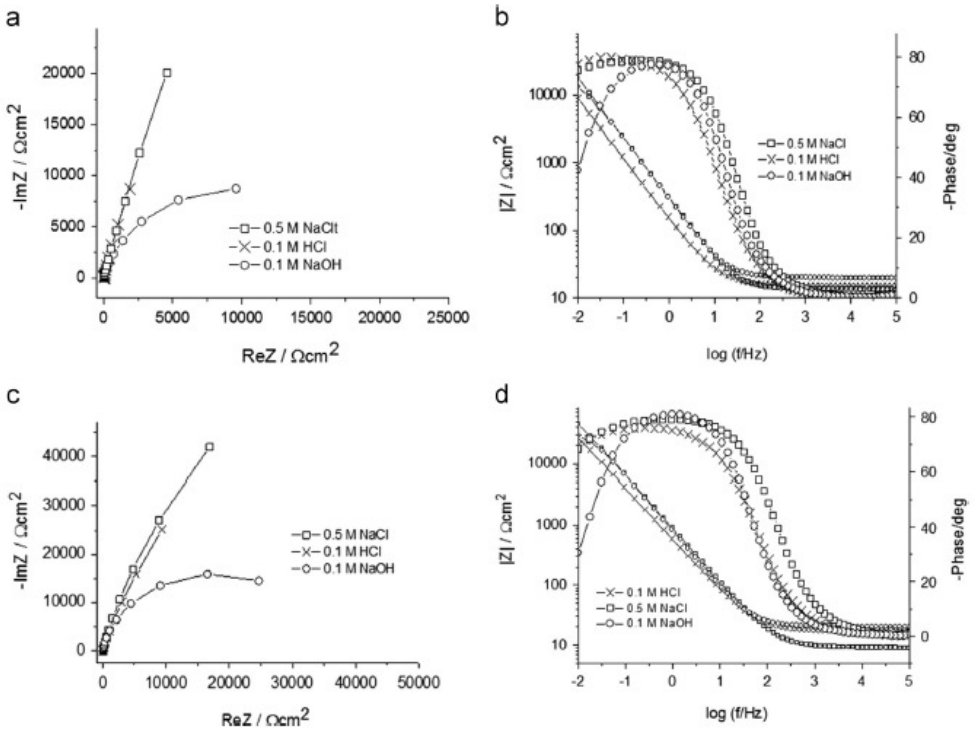

Fig. 8. Electrochemical Impedance data of TiC coated implant materials in three different solutions at open circuit potential (a) TiC/a:C/Ti6Al4V Nyquist plot, (b) TiC/a:C/Ti6Al4V Bode plot, (c) TiC/a:C/CoCrMo Nyquist plot, and (d) TiC/a:C/CoCrMo Bode plot.

The uncoated substrates have superior corrosion resistance to the TiC /a:C coated samples (Fig. 9). One possible explanation may be the compact and homogenous oxide layer formed on the substrate´s surface. The TiO_2 layer is more compact in the case of Ti6Al4V substrate than that the oxide layer formed on CoCrMo surface, according to the Nyquist diagram in Fig. 9a. This fact was shown in [22], too. In the case of Ti6Al4V substrate, the Nyquist diagram shows large capacitive arc. The same plot for CoCrMo substrate bends to the real axis even more and exhibits a large semi-circle like arc. The broad phase angle maximum of Blode plots for all coated and uncoated substrates can be ascribed to two merging phase maximum at medium and low frequency regions commensurate with two overlapping time constants (Fig. 9b).

The fitting quality is evaluated by the chi-squared ($\chi 2$) values, which is about of the order of 10^{-4}, indicating excellent agreement between the measured and the simulated values. The isotonic salt solution presents a low resistance (9-13 Ωcm^2) due to the presence of chloride ions in solution. This magnitude is reasonable because the electrolyte resistance does not interfere with the impedance experiments. The value of R_{ct} is indicative of electron transfer across the interface and reflects the extent of corrosion degradation. These Rct values are higher by about 4 and 7 times for CoCrMo and TiAl6V4 substrates than that of TiC /TiAl6V4 and TiC /CoCrMo samples, respectively. The coating resistances are smaller by

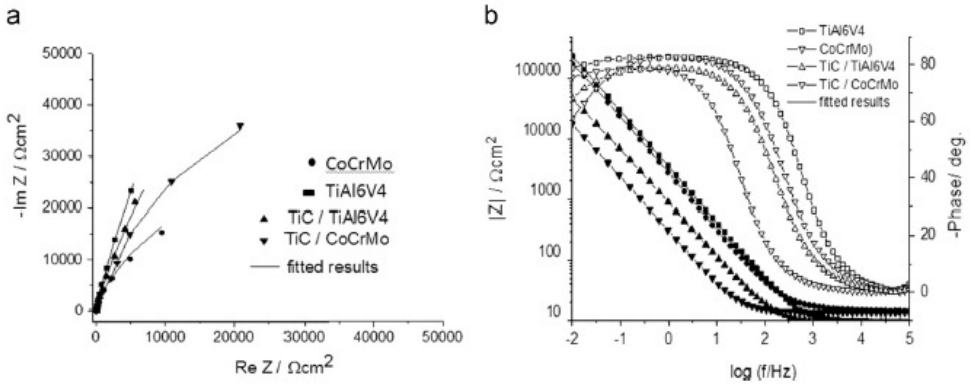

Fig. 9. Plots of impedance spectra for the TiC/a:C coated and uncoated metallic implants in 0.5 M NaCl solution at their respective E_{ocp} (a) Nyquist plots, and (b) Bode plots.

more than 4-5 order of magnitudes than the values of charge transfer resistance in all cases. A smaller coating capacitance values of uncoated samples compared to the TiC /a:C coated ones means that the oxide film formed naturally on the bare samples possesses higher insulating (dielectric) and protecting properties. The variation of CPE values is due to a variation of film thickness or of film dielectric constant. The higher values of CPE suggest a much large surface area, typical of porous layers. The polarization resistance values calculated with Stern-Geary formula from potentiodynamic diagrams were in good agreement with those obtained from impedance measurements.

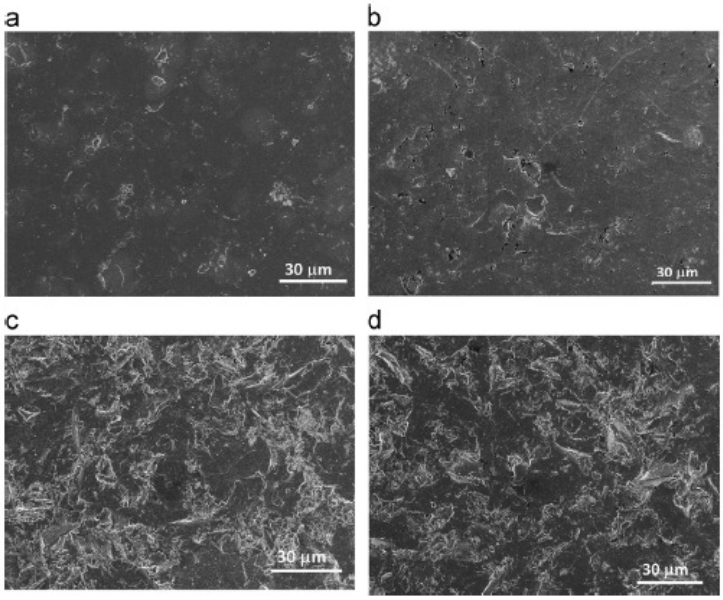

Fig. 10. SEM images corrosion test. (a) TiC/a:C/CoCrMo before corrosion test, (b) TiC/a:C coated CoCrMo after test in 0.1 M NaOH solution, (c) TiC/a:C/ Ti6Al4V before corrosion test, and (d) TiC/a:C coated Ti6Al4V after test in 0.1 M NaOH solution.

3.3 Surface morphology examinations by Scanning Electron Microscopy (SEM)

The SEM investigations before and after corrosion tests were applied for better understanding of influence of solution with different pH values (Fig. 10). It is clearly shown that the roughness of surfaces was changed after the application of the solutions. Fig. 10a illustrates the surface morphology of TiC /a:C coated CoCrMo substrate before the corrosion test. The largest morphological changes found in the 0.1 M NaOH solution (Fig. 10b). Due to

this solution, 10 – 15 µm sized recesses were detected. The effect of other two solutions on the TiC /a:C surface is similar (not shown). A few 10 µm alterations can be observed after the reaction with NaCl solution. SEM images of TiC /a:C coated Ti6Al4V substrate are shown in Fig. 10c, d. It can be concluded that the morphology of TiC /a:C coated substrate before and after corrosion test are very similar. According to the EIS spectra and Nyquist plots, the most prone corrosion effect was observed after the treatment in the 0.1M NaOH solution (Fig. 10d) compared with the measurements in 0.5 M NaCl and 0.1 M HCl solutions (SEM images are not shown).

Sampl.	**uncoated Ti 6Al 4V**			**TiC / Ti 6Al 4V**			**uncoated CoCrMo**			**TiC / CoCrMo**		
solution	0.1M HCl	0.5M NaCl	0.1M NaOH	0.1M HCl	0.5M NaCl	0.1M NaOH	0.1M HCl	0.5M NaCl	0.1M NaOH	0.1M HCl	0.5M NaCl	0.1M NaOH
pH	1	6	13	1	6	13	1	6	13	1	6	13
icorr/ nAcm^{-2}	40.4	5.61	89.0	813	45.1	1595	139	39.8	187	399	108	1002

Tab.1.*Corrosion resistance of the uncoated and* TiC/a:C *coated Ti6Al4V and CoCrMo substrates in three different solutions.*

Conclusions

The TiC /a:C coating with ~ 400 nm thickness was deposited on CoCrMo and Ti6Al4V substrates by DC magnetron sputtering. The 25 nm columnar TiC crystals separated by 2 nm thin carbon matrix layers were observed by TEM investigations for Ti6Al4V substrate. The thin carbon interlayer and different crystalline phase of CoCrMo substrates caused the growth of two times thicker TiC crystals.

The corrosion properties were measured for uncoated and TiC /a:C coated substrates in three different solutions; 0.5 M NaCl solution (pH=6), 0.1 M HCl solution (pH=1) and 0.1 M NaOH solution (pH=13). The best corrosion properties were observed by potentiodynamic measurements and supported by Nyquist and Bode plots in the case of uncoated Ti6Al4V implant. In all cases, the alkaline 0.1 M NaOH solution had the most corrosive effect. This is evidenced by the SEM, which is that the largest morphological changes found in the 0.1 M NaOH solution, too. The Ti6Al4V uncoated substrate showed the highest corrosive resistance under the influence of the 0.5 M NaCl solution.

In conclusion, the uncoated implant showed a better corrosive resistance compared with the TiC /a:C coated substrates. However, the stable and mechanically strong TiC /a:C coating may have a passivation effect and may provide a longer lifetime of implants in the body. These conditions are achievable with producing a TiC /a:C protective film on metal devices.

Acknowledgements

This work was supported by the Hungarian Scientific Research Fund OTKA Postdoctoral grant Nr. PD 101453 and OTKA 105355, the JánosBolyai Research Scholarship of the

Hungarian Academy of Sciences and TéT HU-RO_2012_0006. NikolettOláh thanks to FIKU. The authors are grateful to LeventeIllés for performing SEM measurements.

References

[1] N.T.C. Oliveira, G. Alexio, R. Caram, A.C. Guastaldi, Development of Ti-Mo alloys for biomedical applications: Microstructure and electrochemical characterization, Mat. Sci. Eng. A 452-453 (2007) 727-731.
[2] Z. Doni, A.C. Alves, F. Toptan, J.R. Gomes, A. Ramalho, M. Buciumeanu, L. Palaghian, F.S. Silva, Dry sliding and tribocorrosion behaviour of hot pressed CoCrMo biomedical alloy as compared with the cast CoCrMo and Ti6Al4V alloys, Mater. Des. 52 (2013) 47-57.
[3] M.A.-H. Gepreel, M. Niinomi, Biocompatibility of Ti-alloys for long-term implantation, J. Mech. Behav. Biomed. Mater.20 (2013) 407-415.

[4] J.E.G. González, J.C. Mirza-Rosca, Study of the corrosion behavior of titanium and some of its alloys for biomedical and dental implant applications, J. Electroanal. Chem. 471 (1999) 109-115.

[5] A.M. Soufiani, F. Karimzadeh, M.H. Enayati, Formation mechanism and characterization of nanostructured Ti6Al4V alloy prepared by mechanical alloying, Mater. Des. 37 (2012) 152-160.

[6] I. Gurappa, Characterization of different materials for corrosion resistance under simulated body fluid conditions, Mater. Char. 49 (2002) 73-79.

[7] H. Oudadesse, J.L. Irigaray, E. Chassot, Detection of metallic elements migration around a prosthesis by neutron activation analysis and by the PIXE method, J. Trace Microprobe Tech. 18 (2000)505–510.

[8] S. Wu, X. Liu, K.W.K. Yeung, H. Guo, P. Li, T. Hu, C.Y. Chung, P.K. Chu, Surface nano-architectures and their effects on the mechanical properties and corrosion behavior of Ti-based orthopedic implants, Surf.Coat. Technol. 233 (2013) 13-26.

[9] I. Gurappa, Characterization of titanium alloy Ti-6Al-4V for chemical, marine and industrial applications, Mater. Char. 51 (2003) 131-139.

[10] A.J. Perry, Ion implantation of titanium alloys for biomaterial and other applications, Surf. Eng. 3 (1987) 154-160.

[11] A. Piattelli, A. Scarano, M. Piattelli, Calabrese L, Direct bone formation on sand-blasted titanium implants: an experimental study, Biomaterials 17 (1996) 1015-8.

[12] W.-C. Chen, Y.-S. Chen, C.-L.Ko, Y. Lin, T.-H. Kuo, H.-N. Kuo, Interaction of progenitor bone cells with different surface modifications of titanium implant, Mat. Sci. Eng. C 37 (2014) 305-313.

[13] H.B. Wen, J.R. de Wijn, F.Z. Cui, K. de Groot, Preparation of bioactive Ti6Al4V surfaces by a simple method, Biomaterials 19 (1988) 215-221.

[14] T. Hanawa, In vivo metallic biomaterials and surface modification, Mat.Sci. Eng. A 267 (1999) 260-266.

[15] H. Liu, D. Zhang, F. Shen, G. Zhang, S. Song, Corrosion and ion release behavior of Cu/Ti film prepared via physical vapor deposition in vitro as potential biomaterials for cardiovascular devices, Appl. Surf. Sci. 258 (2012) 7286-7291.

[16] K. Sedláčková, R.O. Grasin, T. Ujvári, I. Bertóti, G. Radnóczi, Carbon-metal (Ni or Ti) nanocomposite thin films for functional applications, Solid State Sci. 11 (2009) 1815-1818.

[17] A. Shanaghi, P.K. Chu, A.R. SabourRouhaghdam, R. Xu, T. Hu, Structure and corrosion resistance of Ti/TiC coatings fabricated by plasma immersion ion implantation and deposition on nickel-titanium, Surf. Coat. Tech. 229 (2013) 151-155.

[18] K. Balázsi, I.E. Lukács, S. Gurbán, M. Menyhárd, L. Bacáková, M. Vandrovcová, C. Balázsi, Structural, mechanical and biological comparison of TiC and TiCN nanocomposites films, J. Eur. Ceram. Soc. 33 (2013) 2217-2221.

[19] K. Balázsi, M. Vandrovcová, L. Bačáková, C. Balázsi, I. Bertóti, F. Davin and G. Radnóczi, Mechanical behavior of bioactive TiC nanocomposite thin films, Mater. Sci. Forum 729 (2013) 296-301.

[20] V. Swaminathan, H. Zeng, D. Lawrynowicz, Z. Zhang, J.L. Gilbert, Electrochemical investigations of chromium nanocarbide coated Ti-6Al-4V and Co-Cr-Mo alloy substrates, Electrochim. Acta 59 (2012) 387-397.

[21] Y. Liao, E. Hoffman, M. Wimmer, A. Fischer, J. Jacobs and L. Marks, CoCrMo metal-on-metal hip replacements, Phys. Chem. Chem. Phys 15 (2013) 746-756.

[22] K. Sedláčková, R. Grasin, G. Radnóczi, Carbon-metal (Ni-Ti) nanocomposite films as protective coatings, in: LM Krause (Ed.), New research on nanocomposites, Nova Pls., New York, 2008, pp. 223-246.

[23] C. Balagna, S. Spriano, M.G. Faga, Characterization of Co–Cr–Mo alloys after a thermal treatment for high wear resistance, Mat. Sci. Eng. C 32 (2012)1868-1877.

[24] J.L. Lábár, Electron Diffraction Based Analysis of Phase Fractions and Texture in Nanocrystalline Thin Films, Part I: Principles, Microsc. Microanal. 14 (4) (2008) 287-295.

[25] J.L. Lábár, Electron Diffraction Based Analysis of Phase Fractions and Texture in Nanocrystalline Thin Films, Part II: Implementation, Microsc. Microanal. 15 (1) (2009) 20-29.

[26] J.L. Lábár, M. Adamik, B.P. Barna, Zs. Czigány, Zs. Fogarassy, Z.E. Horváth, O. Geszti, F. Misják, J. Morgiel, G. Radnóczi, G. Sáfrán, L. Székely and T. Szüts, Electron Diffraction

Based Analysis of Phase Fractions and Texture in Nanocrystalline Thin Films, Part III: Application Examples, Microsc. Microanal. 18 (3) (2012) 406-420.

[27] J.L. Lábár: Consistent indexing of a (set of) SAED pattern(s) with the ProcessDiffraction program, Ultramicroscopy, 103 (2005) 237-249.

[28] Y. Okazaki, E. Gotoh, Metal release from stainless steel, Co-Cr-Mo-Ni-Fe and Ni-Ti alloys in vascular implants, Corros. Sci. 50 (2008) 3429-3438.

[29] L.J. Huang, L. Geng, H.Y. Xu, H.X. Peng, In situ TiC particles reinforced Ti6Al4V matrix composite with a network reinforcement architecture, Mat. Sci. Eng.A 528 (2011) 2859-2862.

[30] A. Dalmau, V.G. Pina, F. Devesa, V. Amigó, A.I. Muñoz, Influence of fabrication process on electrochemical and surface properties of Ti-6Al-4V alloy for medical applications, Electrochim. Acta 95 (2013) 102-111.

[31] D. Durgalakshmi, M. Chandran, G. Manivasagam, M.S. Ramachandra Rao, R. Asokamani, Studies on corrosion and wear behavior of submicrometric diamond coated Ti alloys, Tribol. Int. 103 (3) (2005) 237-249.

[32] Y. Okazaki, Effect of friction on anodic polarization properties of metallic biomaterials, Biomaterials 23 (2002) 2071-2077.

[33] R.W.-W. Hsu, C.-C.Yang, C.-A.Huang, Y.-S. Chen, Electrochemical corrosion studies on Co-Cr-Mo implant alloy in biological solutions, Mater. Chem. Phys. 93 (2005) 531-538.

[34] R.W.-W. Hsu, C.-C.Yang, C.-A.Huang, Y.-S. Chen, Investigation on the corrosion behavior of Ti-6Al-4V implant alloy by electrochemical techniques, Mater. Chem. Phys. 86 (2004) 269-278.